Electronic supplementary information (ESI)

Video S1: Stationary images of a rotating *LabDisk with switch*, recorded by the *strobe LabDisk player*.

The video shows the switching of liquid into collection chamber A (Fig. 2, A.1, manuscript) using the same *LabDisk with switch* as in ESI Video S2. The rotational frequency (indicated in the lower left corner) was kept at 15 Hz while cooling down from 60 °C (after holding for 60 s) to 30 °C.

Video S2: Stationary images of a rotating *LabDisk with switch*, recorded by the *strobe LabDisk player*.

The video shows the switching of liquid into collection chamber B (Fig. 2, B.1-3, manuscript) using the same *LabDisk with switch* as in ESI Video S1. The rotational frequency (indicated in the lower left corner) was first kept at 40 Hz while cooling down from 60 °C (after holding for 60 s) to 30 °C. After 15 s, the rotational frequency was lowered to 9 Hz.

Experimental Details S1: Temperature-dependent dynamic viscosity of air

The dependency of the dynamic viscosity $\eta(T(t))$ of the temperature $T(t)$ (in K) for gases is described by the Sutherland's formula,

$$\eta(T(t)) = \eta_0 \frac{T_0 + S}{T(t) + S} \left(\frac{T(t)}{T_0}\right)^{3/2} \quad \text{(S1A)}$$

where $\eta_0 = 18.27\ 10^{-6}$ Pa s, $T_0 = 291.15$ K, and S = 120 K for air [1].

Experimental Details S2: Geometric factor for fluidic resistance

The geometric factor for calculation of the fluidic resistance is calculated as follows [2] (pages 48-51),

$$K = 1 - \sum_{n=1}^{\infty} \frac{1}{(2n-1)^5} \frac{192}{\pi^5} \frac{\min(w_{fl}, d_{fl})}{\max(w_{fl}, d_{fl})} \tanh\left((2n-1)\frac{\pi}{2}\frac{max(w_{fl}, d_{fl})}{min(w_{fl}, d_{fl})}\right) \quad \text{(S2A)}$$

where w_{fl} is the width and d_{fl} is the depth of the venting resistor. Min(w_{fl},d_{fl}) indicates the smaller value of w_{fl} and d_{fl}. Max(w_{fl},d_{fl}) indicates the greater value of w_{fl} and d_{fl}.

Experimental Details S3: Model verification

The model was verified using eqn (6) (manuscript), which states that the thermally induced underpressure $\Delta p(t)$ inside the collection chamber may be determined by measuring the capillary and centrifugal pressures in the system (at a known ambient pressure). For this, two identical *LabDisks for model verification* (segments) together with a rotary temperature measurement system [3] (TMS) were mounted on a rotor for processing inside the *strobe RGQ* (Fig. S3A).

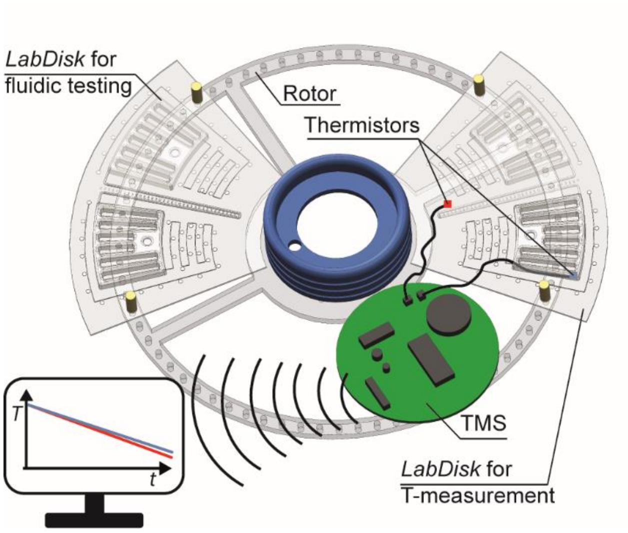

Fig. S3A Experimental set-up for verification of the analytical model including a temperature measurement system (TMS) for measurement under rotation. The TMS is mounted onto a rotor, which holds two identical *LabDisks for model verification* (segments). One segment serves for temperature measurement and thus includes thermistors of the TMS (dimension: 0.6 mm x 0.3 mm x 0.3 mm). Data of the TMS is wirelessly transferred to a computer. Inside the other segment, the fluidic experiment is performed.

The inlet chamber of the segment for fluidic testing was filled with 200 µl deionized water and observed by image acquisition, the other empty segment served for temperature measurement using the TMS. Due to the thermal masses of the thermistors of the TMS, it was found most suitable to use a weighted average of the data from the thermistor inside ($T_i(t)$) and the thermistor outside ($T_o(t)$) of the collection chamber to estimate the actual air temperature $T(t)$ inside the collection chamber as follows,

$$T(t) = 0.6\,T_o(t) + 0.4\,T_i(t) \qquad \text{(S3A).}$$

Prior to the measurement, the rising channel of the siphon was pre-wetted (by cooling down) to prevent biasing of the measurement by pinning of the liquid meniscus. Using ImageJ (National Institutes of Health, Bethesda, MD, USA), the filling heights of the liquid inside the rising siphon channel (A = 385 µm x 385 µm) and inside the inlet chamber were measured to determine the centrifugal pressure difference $\Delta p_{cent}(t)$ (eqn (8), manuscript). Besides, the contact angel of the liquid inside the siphon channel was observed over time to determine the capillary pressure $\Delta p_{cap}(t)$. The corresponding change of contact angle over time $\Theta(t)$ influences on the one hand the measured thermally induced underpressure $\Delta p(t)^{meas}$ (eqn (6), manuscript) and on the other hand the underpressure-dependent volume $V(\Delta p(t))$ (eqn (9), manuscript) and thereby the modeled thermally induced underpressure $\Delta p(t)^{\mathrm{mod}}$ (eqn (5), manuscript). Using $\Delta p_{\mathrm{cent}}(t)$ and $\Delta p_{\mathrm{cap}}(t)$, eqn (6) (manuscript) allows to derive a measured thermally induced underpressure $\Delta p(t)^{\mathrm{meas}}$ inside the collection chamber. In addition, the temperature measurement of the TMS was used to calculate a modeled thermally induced underpressure $\Delta p(t)^{\mathrm{mod}}$ inside the collection chamber by numerically solving eqn (5) (manuscript).

Both variations were cooled at two different TCR: Since the Rotor-Gene Q/*strobe RGQ* does not allow to define the TCR itself, its RGQ Series Software (version 2.1.0 build 9, QIAGEN) was set to cool down to 35 °C starting from two different temperatures, *i.e.* 60 and 50 °C, which effectively results in different TCR. In addition, even though the siphon channel features a crest on the minimal radial position that can still be observed in the *strobe RGQ* (24.6 mm) to characterize a maximum range of pressure changes, the limitation of the constant 400 RPM of the *strobe RGQ* limits the experimental model verification to the characterization of the influence of the TCR $\dot{T}(t)$ and the fluidic resistance R_{fl} and only up to a maximum of 1.92 kPa thermally induced underpressure. Each experimental configuration is tested three times, which adds up to a set of 12 measurements.

Experimental Details S4: Demonstration of applications

The *LabDisk player* features a processing chamber, where either the *LabDisk with switch* or the *sample-to-answer LabDisk* is placed on a rotor mounted on the rotational axis. Upon closing of the lid of the processing device, a rotational frequency protocol and an air-mediated heating and cooling of the processing chamber can be executed. Thus, the *LabDisk player* uses global heating and cooling of the entire *LabDisk* (structures). As enhancement, the *strobe LabDisk player* allows for observation of the liquid flow inside the rotating respective *LabDisk* (Fig. S4A).

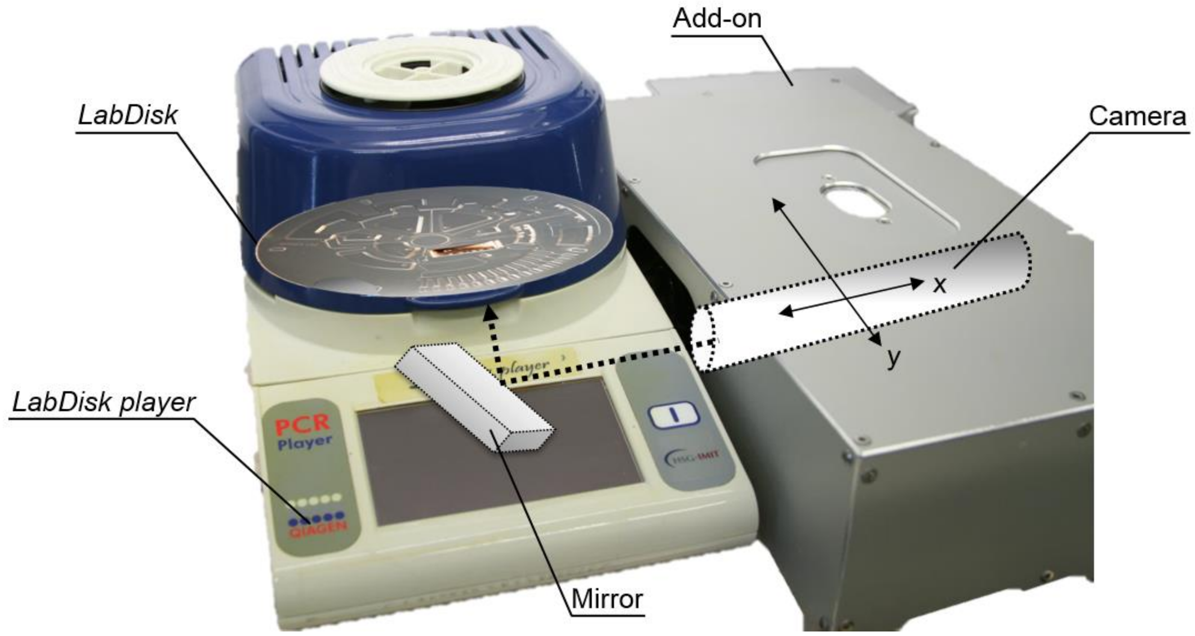

Fig. S4A Experimental set-up of the *strobe LabDisk player*. Liquid flow under rotation is visualized using a camera that acquires picture frames at a defined radial and azimuthal position on the *LabDisk*.

Video S3: Stationary images of a rotating *sample-to-answer LabDisk*, recorded by the *strobe LabDisk player*.

The video shows the valving of liquid from the mixing chamber into the aliquoting structure (Fig. 7, C-D, manuscript). The time in ms is indicated in the upper left corner. At a final cooling step from 70 to 50 °C the TCR actuated siphon valve is robustly actuated by allowing valving at low rotational frequency. Liquid is transferred downstream by centrifugal forces into the aliquoting structure for PCR main-amplification.

References

1 Z. Tan, *Air pollution and greenhouse gases. From basic concepts to engineering applications for air emission control*, Sprinter, Singapore, New York, 2014.

2 H. Bruus, *Theoretical microfluidics*, Oxford University Press, Oxford, 2008, vol. 18.

3 J. Burger et al., *DIRECT ON-DISK WIRELESS TEMPERATURE MEASUREMENT FOR CENTRIFUGAL MICROFLUIDIC PLATFORMS.* Proc. of the 14th International Conference on Miniaturized Systems for Chemistry and Life Sciences (µTAS). 2010, accessed 28 August 2015.